DEMONSTRATING THE NEGLIGIBLE CONTRIBUTION OF OPTICAL *HST* ACS GALAXIES TO SOURCE-SUBTRACTED COSMIC INFRARED BACKGROUND FLUCTUATIONS IN DEEP *SPITZER* IRAC IMAGES

A. KASHLINSKY,[1,2] R. G. ARENDT,[1,2] J. MATHER,[1,3] AND S. H. MOSELEY[1,3]

ABSTRACT

We study the possible contribution of optical galaxies detected with the *Hubble* ACS instrument to the near-IR cosmic infrared (CIB) fluctuations in deep *Spitzer* images. The *Spitzer* data used in this analysis are obtained in the course of the GOODS project, from which we select four independent $10' \times 10'$ regions observed at both 3.6 and 4.5 μm. ACS source catalogs for all of these areas are used to construct maps containing only their emissions in the ACS *B,V,i,z* bands. We find that deep *Spitzer* data exhibit CIB fluctuations remaining after removal of foreground galaxies of a very different clustering pattern at both 3.6 and 4.5 μm than the ACS galaxies could contribute. We also find that there are very good correlations between the ACS galaxies and the *removed* galaxies in the *Spitzer* maps, but practically no correlations remain with the residual *Spitzer* maps used to identify the CIB fluctuations. These contributions become negligible on larger scales used to probe the CIB fluctuations arising from clustering. This means that the ACS galaxies cannot contribute to the large-scale CIB fluctuations found in the residual *Spitzer* data. The absence of their contributions also means that the CIB fluctuations arise at $z \gtrsim 6.5$ as the Lyman break of their sources must be redshifted past the longest ACS band, or the fluctuations have to originate in the more local but extremely low luminosity galaxies.

Subject headings: cosmology: observations — diffuse radiation — early universe

1. INTRODUCTION

The cosmic infrared background (CIB) is comprised of emission from luminous objects from all epochs in the universe, including by those too faint for individual detection by current telescopic studies (see Kashlinsky 2005 for review). A particularly interesting contributor to CIB comes from the first-stars epoch (Santos et al. 2002), which may have left measurable CIB fluctuations (Kashlinsky et al. 2004; Cooray et al. 2004). An attempt to measure this CIB fluctuations component was made recently by Kashlinsky et al. (2005, 2007a, 2007b; hereafter KAMM1, KAMM2, KAMM3) using deep IRAC *Spitzer* images at 3.6–8 μm. The first results used a ~10 hr exposure of a $5' \times 10'$ field from Fazio et al. (2004) and, after removing foreground galaxies to $m_{AB} \sim 25$ (at 3.6 μm), detected an excess CIB fluctuations component over that from the remaining "ordinary" galaxies at $\gtrsim 0.5'$ (KAMM1). KAMM1 showed that the fluctuations do not arise from zodiacal light, Galactic cirrus, or instrumental noise or artifacts (see also KAMM2) and that the residual maps do not correlate with the removed sources. A follow-up study by KAMM2 used much deeper GOODS data (Dickinson et al. 2003) with $\gtrsim 20$ hr exposures in two independent sky areas observed at two epochs. The new data in four independent fields allowed KAMM2 a better removal of foreground galaxies, i.e., until a fixed floor of the residual shot noise contribution to the power spectrum, P_{SN}, was reached. At the same level of P_{SN} all regions have the same large-scale CIB fluctuations, consistent with their cosmological origin. The new measurements allowed a firmer interpretation of the cosmological sources generating these CIB fluctuations: they must have at most a fairly low shot noise component and at the same

time produce a significant CIB fluctuations component at $\gtrsim 0.5'$ arising from clustering (KAMM3).

Recently, Cooray et al. (2007) attempted to demonstrate that the signal detected by KAMM1 at 3.6 μm originates from optical galaxies detected by the *Hubble* ACS instrument. In one of the GOODS regions they blanked the pixels in the IRAC maps corresponding to the optically identified ACS sources and, from the remaining ~20% of the map, evaluated the power spectrum of the diffuse emission claiming that it is significantly attenuated when the ACS sources are removed. It was pointed out by Kashlinsky (2007) that such analysis is flawed: for such deeply cut maps one cannot evaluate clustering properties using Fourier transforms because the basis functions are no longer even approximately orthogonal (e.g., Gorski 1994). Kashlinsky (2007) further demonstrates that when the correlation function, $C(\theta)$, which is immune to masking, is computed instead for the Cooray et al. maps it does not depend, within the statistical uncertainties, on whether or not ACS sources are removed.

In this Letter we present the results from our study of whether the optically detected ACS galaxies can explain the CIB fluctuations detected by KAMM. Because the large-scale fluctuations do not have a high S/N for the longest IRAC channels, where the instrument noise is significant, we restricted our analysis to the 3.6 and 4.5 μm IRAC channels. We note that any explanation of the fluctuations must account for at least the measured amplitude *and* slope at *both* 3.6 and 4.5 μm and at the right level of the shot noise (KAMM3). We show that the galaxies detected in the ACS GOODS survey cannot contribute significantly to the CIB fluctuations detected by KAMM because they produce diffuse light with very different power spectrum properties and, more importantly, there are negligible correlations between the maps used in the KAMM analysis and those of the ACS sources.

2. IRAC DATA AND RESULTS

The GOODS IRAC data used for this investigation are described in KAMM2. Briefly: The GOODS IRAC observations

[1] Observational Cosmology Laboratory, Code 665, Goddard Space Flight Center, Greenbelt, MD 20771; kashlinsky@milkyway.gsfc.nasa.gov, arendt@milkyway.gsfc.nasa.gov, mather@milkyway.gsfc.nasa.gov, moseley@milkyway.gsfc.nasa.gov.
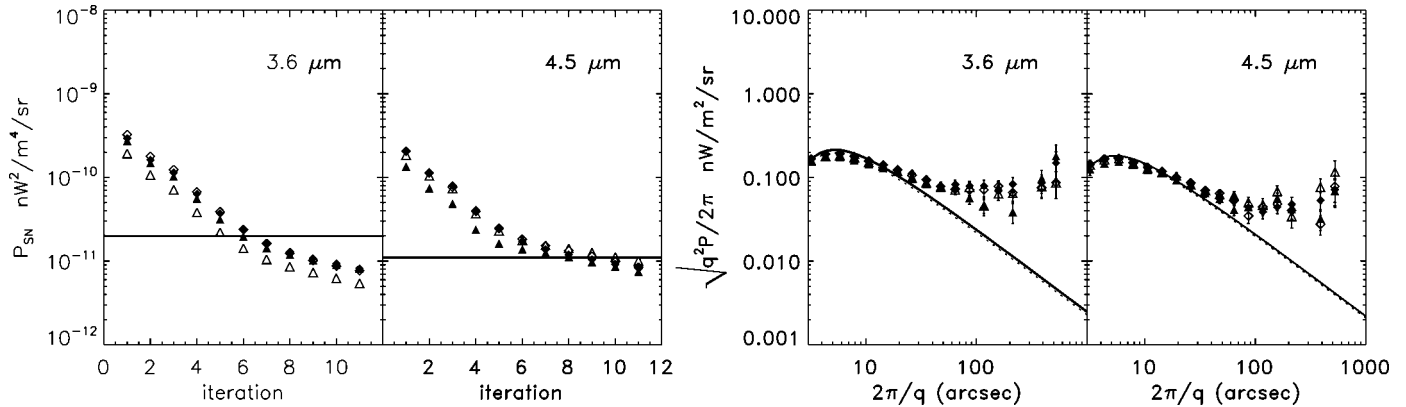[2] SSAI.
[3] NASA.

FIG. 1.—KAMM2 results for the 972 × 972 0.6″ pixel fields. Triangles correspond to the HDFN region, diamonds to CDFS region; open symbols to E1, filled to E2. *Left*: Decrease of the shot noise contribution to the power spectrum vs. the iteration number of the KAMM source model. Horizontal lines show the levels reached in KAMM2, which are a factor of ~2 below those in KAMM1. *Right*: CIB fluctuations from the residual maps used in the present analysis at the shot noise levels of KAMM2.

of the HDF-N and CDF-S fields cover regions roughly $16' \times 10'$ in size. The coverage is obtained through two $10' \times 10'$ mosaics (which overlap by ~4′) that are obtained at epochs ~6 months apart (E1 and E2). For this project the individual Basic Calibrated Data (BCD) frames were self-calibrated using the method of Fixsen et al. (2000), and mosaicked into images with 0.6″ pixels. The self-calibration solves for fixed pattern detector offsets that may be incompletely removed by the BCD pipeline (e.g., diffuse stray light), and for frame-to-frame offset variations. The self-calibration does not remove the intrinsic large-scale power other than that due to (arbitrary) linear gradients, and is particularly useful for studies of the diffuse-light fluctuations. Self-calibration cannot find a consistent solution if both epochs are combined, because variation in the intensity, and especially the direction of the gradient, of the zodiacal light invalidate the assumption that the sky itself is a stable calibration source on 6 month timescales. Thus, our analyzed regions are four independent subfields of $583'' \times 583''$ in size with common coverage at both 3.6 and 4.5 μm. We refer to them below as HDFN-E1, HDFN-E2, CDFS-E1, and CDFS-E2.

The assembled data were cleaned of resolved sources in two steps: (1) An iterative procedure was applied whereby each iteration calculates the standard deviation (σ) of the image, and then masks all pixels exceeding $N_{cut} \sigma$ along with $N_{mask} \times N_{mask}$ surrounding pixels. The procedure is repeated until no pixels exceed $N_{cut} \sigma$. The clipping parameters were fixed so that enough pixels ($\gtrsim 70\%$) remain for robust Fourier analysis. As in the early DIRBE work (Kashlinsky & Odenwald 2000) the blanked pixels were set to zero, and the resulting power spectrum was divided by the fraction of nonzero pixels in the image, thereby preserving the total power of the noise. (2) At the second stage we removed a model of the individual sources described in KAMM1. This is done using a variant of the CLEAN algorithm (Högbom 1974). The process identifies the brightest pixel in the image, and then subtracts a scaled PSF at that location to remove a fixed fraction of the flux. This is repeated many thousands of times until the components being subtracted are comparable to the noise level of the images. Intermediate results are saved after each "iteration," consisting of the subtraction of ~10^4 components. As progressively fainter sources are removed with each iteration, the shot noise from the remaining galaxies decreases as does their contribution to large-scale power.

Comparison of the different regions is most direct if the source cleaning is halted at the same specified level of P_{SN}. Figure 1 (*left*) shows the decrease of P_{SN} with each iteration of the cleaning procedure for the four regions used in the study. The right panels in Figure 1 show the CIB fluctuations derived for the marked level of P_{SN} used in KAMM2. One can see the excess over the shot noise at scales $\gtrsim 0.5'$. It is important to emphasize that the fluctuations have the large-scale power spectrum, $P(q) \propto q^{-n}$, such that the amplitude of fluctuations is approximately flat to slowly rising with scale, corresponding to the effective index $n \gtrsim 2$.

3. ACS GALAXIES AND THEIR FLUCTUATIONS

We now evaluate the diffuse light fluctuations that ACS galaxies would generate in the IRAC maps. For this we constructed synthetic maps over the same regions of the sky at 3.6 and 4.5 μm using the *HST*-ACS GOODS catalogs (ver. 1.1z; Giavalisco et al. 2004). These were used to generate images of the observed *B*, *V*, *i*, and *z*-band galaxy distributions that are free of (1) small-scale noise and (2) intrinsically large-scale features, whether due to a diffuse or unresolved astronomical component or low-level instrumental calibration artifacts. The process for each ACS band was as follows: First, four blank images with the same scale and orientation of the IRAC images were generated for the HDFN-E1 and E2 and CDFS-E1 and E2 regions. Then, for each cataloged source, the SExtractor (Bertin & Arnouts 1996) parameters THETA_IMAGE, A_IMAGE, and B_IMAGE were used to define a normalized Gaussian shape and orientation for each source, except for "stellar" sources (CLASS_STAR > 0.9), which were represented as a single pixel. The intensity of each source was scaled to fit the MAG_BEST magnitude, and each source was added to the initially blank image at the location designated by the ALPHA_J2000 and DELTA_J2000 parameters. Finally, for comparison with the IRAC data, each of these images of the catalog sources was convolved with the 3.6 μm or 4.5 μm PSF, as appropriate. For each of the four fields and at both 3.6 and 4.5 μm, we prepared one image containing all ACS sources, and four others that included only ACS sources fainter than set AB magnitude limits (m_0, $m_0 + 2$, $m_0 + 4$, $m_0 + 6$) with $m_0 = (21.8, 21.8, 21.1, 20.6)$ in the ACS *B*,*V*,*i*,*z* bands.

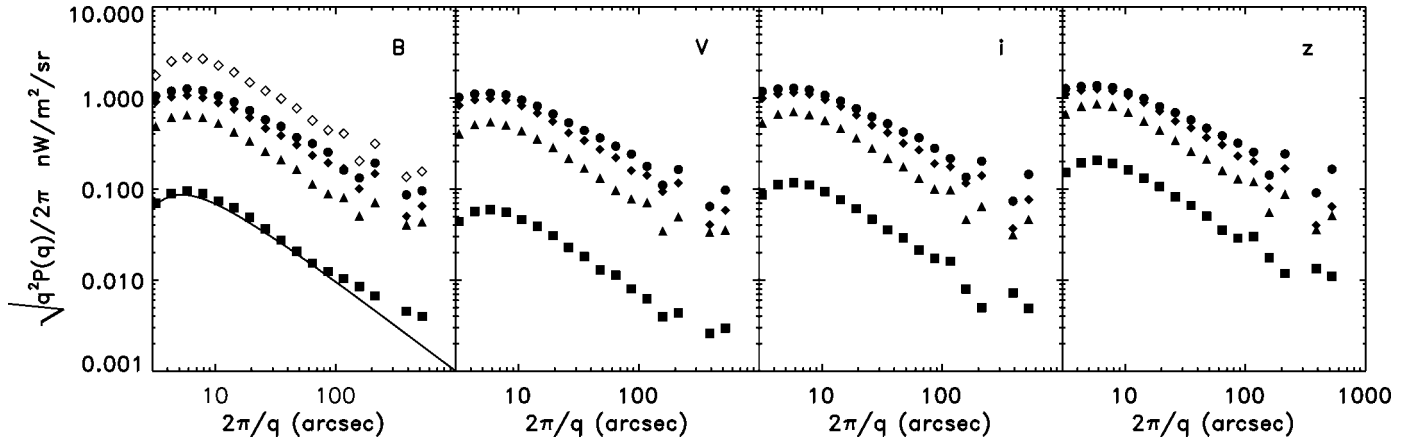After the synthetic maps of ACS sources were prepared, they

FIG. 2.—The fluctuations produced by ACS galaxies for the 972 × 972 0.6″ pixel field at HDFN-E2 region. Filled circles correspond to ACS galaxies fainter than $m_0 = (21.8, 21.8, 21.1, 20.6)$ with the mask defined by the clipping. Filled diamonds, triangles, and squares correspond to fluctuations produced by sources fainter than $m_0 + 2$, $m_0 + 4$, $m_0 + 6$. Open diamonds in the *B*-band panel show the fluctuations produced by galaxies fainter than $m_{AB} = 23.8$ when the clipping mask is not applied; the symbols show that such galaxies were effectively removed from the ACS maps by clipping alone done in KAMM. Solid line shows the shot noise slope corresponding to the faintest galaxies. It is clear that ACS galaxies are clustered, but the effective index of the clustering becomes closer to $n \sim 0$ for fainter samples, in general agreement with Fig. 2 of Kashlinsky et al. (2002).

were masked using the template derived from clipping (step 1 above) of the IRAC data. Figure 2 shows the fluctuations due to galaxies at all ACS wavelengths in the HDFN-E2 region (others are similar to within statistical uncertainties). Fluctuations of these *masked* maps show little difference out to a certain magnitude, which means that the clipping of IRAC data takes out galaxies very accurately for $m_{AB} > 23$–24 in *B*,*V*,*i*,*z*-band ACS filters. The power spectrum of the remaining sources is very different from that of the KAMM CIB fluctuations: it has effective index $n \lesssim 0.5$ and is very similar to the spectrum of CIB fluctuations detected in the deep 2MASS data by Kashlinsky et al. (2002) and Odenwald et al. (2003). The latter arises from galaxies fainter than $K_{Vega} \simeq 19$ ($m_{AB} \sim 21$ at 2.2 μm), which are located at $z \sim 1$ (Cirasuolo et al. 2007), as are the bulk of the ACS galaxies. On the other hand the slope of the fluctuations in Figure 1 (*right*) is described well by the concordance ΛCDM model at high z (KAMM3). The differently sloped power spectra at large scales indicate that the resolved ACS galaxies are unlikely contributors to the large-scale 3.6 and 4.5 μm fluctuations.

The amplitude of the fluctuations at large scales is also small. Indeed the most that the ACS galaxies can contribute to the residual KAMM maps is constrained by the amount of the small-scale shot noise power measured to give fluctuations at a few arcseconds of order $\sim$0.2 nW m^{-2} sr^{-1} at both 3.6 and 4.5 μm. Scaling the numbers in Figure 2 by the corresponding amount would then give contributions from the remaining ACS sources at arcminute scale well below the levels measured by KAMM and shown in Figure 1 (*right*). This by itself implies that the KAMM CIB fluctuations cannot arise in the ACS galaxies.

4. CROSS-CORRELATING ACS AND IRAC DATA

If the ACS galaxies were to explain the KAMM signal there would need to be a strong correlation between the ACS source maps and KAMM maps, and their cross-correlation function would have to exhibit the same behavior at scales larger than the IRAC beam. We computed both the correlation coefficients, $R_0 = \langle \delta F_{ACS} \delta F_{KAMM} \rangle / \sigma_{ACS} \sigma_{KAMM}$, and the full cross-correlation matrix, $C(\theta) = \langle \delta F_{ACS}(x) \delta F_{KAMM}(x + \theta) \rangle$, between the ACS and KAMM maps.

Figure 3 (*left*) shows a very good correlation between the IRAC sources removed by our modeling and the sources in the ACS catalog. On the other hand, only very small correlations (of order a few percent) remain between the residual KAMM maps, containing the fluctuations in Figure 1 (*right*), and the ACS sources. These correlation coefficients also remain quite small as one subselects maps made only with progressively fainter ACS sources.

To further test contributions of ACS galaxies to fluctuations on scales greater than the IRAC beam, we computed the correlation function $C(\theta)$ versus the separation angle θ. In this representation, the contributions of any white-noise (such as shot noise and/or instrument noise) component to $C(\theta)$ drop off very rapidly outside the beam and for the IRAC 3.6 μm channel contribute negligibly to the correlation function at θ greater than a few arcseconds. This is best seen from the analog of the correlation coefficient at nonzero lag, defined as $R(\theta) \equiv C(\theta)/\sigma_{ACS}\sigma_{KAMM}$. This quantity is shown in the right panels of Figure 3 using the example of the CDFS-E2 region. The mean square fluctuation on scale θ is given by the integral $\langle \delta F(\theta)^2 \rangle = (2/\theta^2) \int_0^\theta C(\theta')\theta'd\theta'$ (e.g., Landau & Lifshitz 1958). Hence, we evaluated from $R(\theta)$ a related quantity $\mathcal{R}(\theta) = (2/\theta^2) \int_0^\theta R(\theta')\theta'd\theta'$, shown in the bottom right panels in Figure 3. The correlations are negligible outside the IRAC beam, which means that, at most, the remaining ACS sources contribute to the shot noise levels in the residual KAMM maps (as discussed by KAMM3), but not to the large-scale correlations in Figure 1 (*right*).

5. CONCLUSIONS

Our analysis shows that the source-subtracted CIB fluctuations detected recently by KAMM in deep *Spitzer* images cannot originate in the optical galaxies seen in the GOODS ACS data. While the *B*,*V*,*i*,*z*-band galaxies are well correlated with those seen *and removed* in the 3.6 and 4.5 μm data, they correlate poorly with the residual 3.6 and 4.5 μm background emission. These galaxies also exhibit a very different spatial power spectrum than the KAMM maps and the amplitude of their fluctuations is generally also low. Thus, as discussed in KAMM3, the distant "ordinary" galaxies contribute to the shot noise component of the fluctuations, but their contribution to
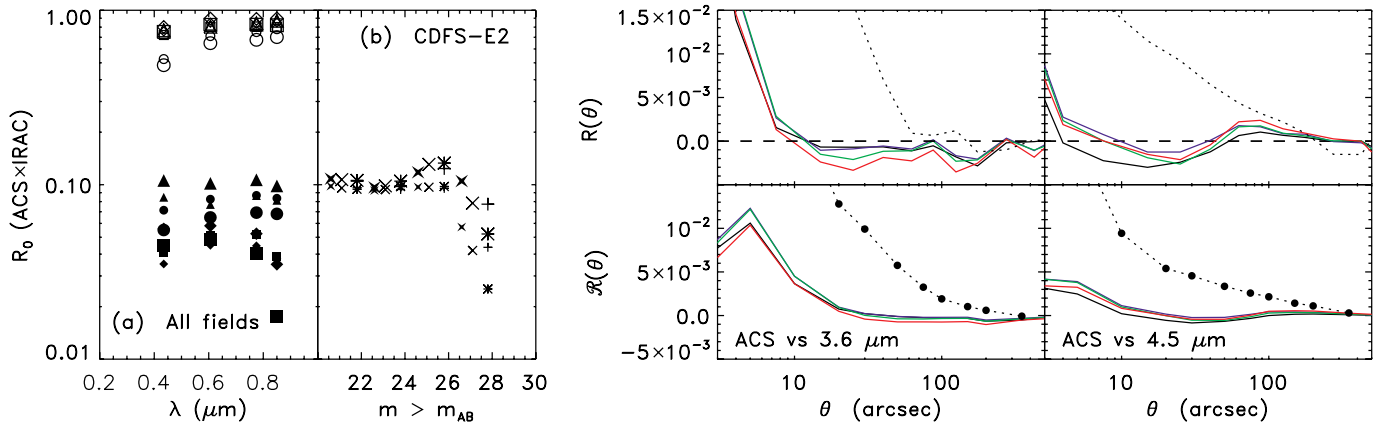
Fig. 3.—*Left*: Correlation coefficient between clipped/masked ACS and KAMM data. Large and small symbols correspond to the IRAC channel 1 (3.6 μm) and channel 2 (4.5 μm). (*a*) The correlation coefficient when *all* ACS catalog sources are included. Open symbols correspond to correlations with the maps of the removed sources and filled symbols with the residual KAMM maps that contain the fluctuations shown in Fig. 1. Circles, diamonds, triangles, and squares correspond to HDFN-E1, HDFN-E2, CDFS-E2, and CDFS-E2. In some areas of the sky, such as CDFS-E2, a few bright sources (both galaxies and Galactic stars at $m_{AB} \lesssim 21$) can noticeably reduce the correlation coefficient. (*b*) Correlation coefficient with the ACS maps that include only sources *fainter* than the magnitude shown in the horizontal axis. Asterisks, pluses, crosses, and the four-pointed stars correspond to the maps using ACS B,V,i,z sources. *Right*: Black, blue, green, and red solid lines show the dimensionless correlation function between the diffuse light in the ACS and KAMM maps for the B,V,i,z bands. Dotted line shows the dimensionless correlation function of the KAMM maps, $C_{KAMM}(\theta)/\sigma^2_{KAMM}$, which remains positive out to ~100" and is better viewed when presented in log-log plots, as in Fig. SI-4 of KAMM1. The dashed horizontal line marks $R = 0$. The bottom panels show a more direct measure of the fluctuations on a given scale, $\mathcal{R}(\theta) = (2/\theta^2) \int_0^\theta R(\theta')\theta'd\theta'$.

the clustering component is at most small. The amplitude of the KAMM source-subtracted CIB fluctuations requires significant CIB fluxes from objects fainter than the KAMM subtraction limit. Deep galaxy counts do not show signs of turning over at faint magnitudes, but their cumulative CIB levels saturate at magnitudes well below the KAMM removal threshold (Madau & Pozzetti 2000; Fazio et al. 2004).

Whatever sources are responsible for the KAMM fluctuations, they are not present in the ACS catalog. There are two ways to reproduce this: (1) Since the ACS galaxies do not contribute to the source-subtracted CIB fluctuations, the latter must arise at $z \gtrsim 6.5$ as is required by the Lyman break at rest ~0.1 μm getting redshifted past the ACS z-band of peak wavelength $\simeq 0.85$ μm. This would place the sources producing the KAMM signal within the first 0.75 Gyr of the evolution of the universe and make conclusions of KAMM3 regarding their

very low M/L stronger. (2) Alternatively, the KAMM fluctuations would have to originate in lower z galaxies that escaped the ACS GOODS source catalog either because they have low surface brightness or are below the catalog flux threshold, but at the same time generate diffuse-light fluctuations of higher amplitude and different slope than the populations already included there. In the latter case we can conservatively estimate their expected luminosities, using the z-band $m_{AB} \gtrsim 24$–26.5 corresponding to the source-size-dependent completeness limit of the ACS catalog (Giavalisco et al. 2004). Such galaxies then would have to be very low luminosity systems since, e.g., for $m_{AB} = 24$ the in-band luminosity corresponding to (B, z) band is $(4, 2) \times 10^7 h^{-2} L_\odot$ at $z = 1$ emitted at rest 0.22, 0.45 μm.

REFERENCES

Bertin, E., & Arnouts, S. 1996, A&AS, 117, 393
Cirasuolo, M., et al 2007, MNRAS, submitted (astro-ph/0609287)
Cooray, A., et al. 2004, ApJ, 606, 611
———. 2007, ApJ, 659, L91
Dickinson, M., et al. 2003, in The Mass of Galaxies at Low and High Redshift, ed. R. Bender & A. Renzini (Berlin: Springer), 324
Fazio, G., et al. 2004, ApJS, 154, 39
Fixsen, D. J., Moseley, S. H., & Arendt, R. G. 2000, ApJS, 128, 651
Giavalisco, M., et al. 2004, ApJ, 600, L93
Gorski, K. 1994, ApJ, 430, L85
Högbom, J. 1974, A&AS, 15, 417
Kashlinsky, A. 2005, Phys. Rep., 409, 361
———. 2007, preprint (astro-ph/0701147)
Kashlinsky, A., Arendt, R., Gardner, J. P., Mather, J. C., & Moseley, S. H. 2004, ApJ, 608, 1

Kashlinsky, A., Arendt, R., Mather, J. C., & Moseley, S. H. 2005, Nature, 438, 45 (KAMM1)
———. 2007a, ApJ, 654, L5 (KAMM2)
———. 2007b, ApJ, 654, L1 (KAMM3)
Kashlinsky, A., & Odenwald, S. 2000, ApJ, 528, 74
Kashlinsky, A., Odenwald, S., Mather, J., Skrutskie, M., & Cutri, R. 2002, ApJ, 579, L53
Landau, L. D., & Lifshitz, E. M. 1958, Statistical Physics (London: Pergamon Press)
Madau, P., & Pozzetti, L. 2000, MNRAS, 312, L9
Odenwald, S., Kashlinsky, A., Mather, J., Skrutskie, M., & Cutri, R. 2003, ApJ, 583, 535
Santos, M. R., Bromm, V., & Kamionkowski, M. 2002, MNRAS, 336, 1082